

# Absolute nodal coordinate formulation of tetrahedral solid element

Alexander Olshevskiy · Oleg Dmitrochenko ·  
Hyun-Ik Yang · Chang-Wan Kim 

Received: 27 February 2016 / Accepted: 28 January 2017 / Published online: 24 February 2017  
© Springer Science+Business Media Dordrecht 2017

**Abstract** A solid tetrahedral finite element employing the absolute nodal coordinate formulation (ANCF) is presented. In the ANCF, the mass matrix and vector of the generalized gravity forces used in the equations of motion are constant, whereas the vector of the elastic forces is highly nonlinear. The proposed solid element uses translations of nodes as sets of nodal coordinates. The tetrahedral shape of the element makes it suitable for modeling structures with complex shapes, and the small number of the degrees of freedom enables good performance and versatile application to problems of structural dynamics. The accuracy and convergence of the element were investigated using statics and dynamics benchmarks and a practical industry application.

**Keywords** Absolute coordinate formulation · Flexible multibody dynamics · Large displacement · Finite element method · Tetrahedral solid element

## 1 Introduction

Numerical simulation is vital to the design and optimization of modern mechanical systems and structures, and there is hardly an area of engineering science in which virtual experiments are not utilized. In numerical simulation, a real-life mechanical system or structure is represented by a numerical model and analyzed using various numerical methods. The broad application of numerical simulation to mechanical systems began with the development of the finite element method (FEM) [1] in the middle of the twentieth century. Most mechanical systems can be considered as multibody systems; that is, a combination of rigid and flexible bodies connected by joints and subjected to external loads. Very often, mechanical systems undergo large overall translation and rotation as well as large deformations. Examples of such structures can be found in many areas. Belt drives, mooring systems, helicopter blades, caterpillars, pantograph, and vehicle airbags are the types of systems and structures dealt with in mechanical engineering, whereas biomechanics researchers investigate insect wings, soft tissues, cardiac implants, and blood vessels. The analysis of such systems necessitates the formulation of equations of motion, which can be highly nonlinear and require numerical solution.

There are several methods that can be used for the numerical simulation of flexible multibody systems. An example is the *floating frame of reference formu-*

---

A. Olshevskiy · C.-W. Kim (✉)  
School of Mechanical Engineering, Konkuk University,  
Seoul 143-701, Korea  
e-mail: goodant@konkuk.ac.kr

O. Dmitrochenko  
Research Department, Bryansk State Technical University,  
7, Bulv. 50 Let Oktyabrya, Bryansk, Russia 241035

H.-I. Yang  
Department of Mechanical Engineering, Hanyang University,  
Ansan 426-791, Korea

lation (FFRF) [20]. In the FFRF, the position of an arbitrary point on a body is decomposed into a rigid body motion and small deformation. The rigid body motion is described in the global reference frame, while the deformation is defined in a local coordinate system. The Coriolis and centrifugal inertia terms produce a highly nonlinear mass matrix and generalized gravity forces. The stiffness matrix of the system is constant for infinitely small deformations and a linear material. FFRF cannot be used to simulate large deformations. FFRF is often compared to the absolute nodal coordinate formulation (ANCF), which is a state-of-the-art finite element technique introduced by Shabana for simulating the large deformations of flexible systems accompanied by a large overall motion [2,3]. In the ANCF, the large displacements of the body are described in the global reference frame without the use of any local reference frame, and the absolute coordinates of the nodes and their spatial derivatives are used as sets of the nodal degrees of freedom of the element. Rotational degrees of freedom are not used, and the shape of an element is described based on global slopes. The nonuse of local reference frames in the ANCF means that there are no gyroscopic effects. Hence, the mass matrix for both linear and nonlinear problems and the vector of the generalized gravity forces are constant, whereas the centrifugal and Coriolis inertia forces vanish. However, the vector of the elastic forces remains nonlinear even when linear strain–displacement relationships are used. These conditions may cause the expressions defining the vector of the elastic forces to be quite complex and cumbersome.

Many finite elements based on the ANCF have been developed by researchers. The vast majority of the literature on the ANCF is devoted to the formulation of beam [4–14] and plate/shell elements [15–25] with different kinematic properties. A detailed review of the literature on ANCF was undertaken by Gerstmayr et al. [26]. However, relatively little attention has been paid to solids. This is not as surprising as it might initially appear. Although ANCF is rapidly developing, it is still a relatively new method. Its application to beams and plates has some definite benefits, and most flexible engineering structures have shapes that fit well with classical beam and plate/shell assumptions. Indeed, ANCF beams with the desired kinematic features can be easily used to represent long flexible structures with certain cross sections while maintaining the proper-

ties of the real-life mechanical system. This can even be achieved by means of a relatively small number of elements in the model, whereas the detailed modeling of 3D solid structures always requires many elements. However, until recently, the use of large ANCF models caused severe computational difficulties, especially for high-order elements with many degrees of freedom. These circumstances, in our opinion, partially explain why 3D solid ANCF elements have so far not been well developed.

Nevertheless, the use of ANCF to develop solid elements is of considerable academic and practical interest because new elements potentially have broad applications in various engineering fields. Most conventional finite elements that are of interest for engineering calculations were developed a long time ago and are well described in the literature [1–3]. It has been shown that most existing elements can be transformed into ANCF elements [27,28]. They can also be developed from scratch and used as isoparametric elements. With the increased computational power of state-of-the-art computers, the use of the ANCF versions of some conventional solid elements looks promising.

Kübler et al. proposed a formulation of multibody systems wherein flexible bodies are described using absolute coordinates for isoparametric hexagonal elements [29]. There is the opinion that, because ANCF originated from elements with slopes [3], it can be implicitly assumed that elements without slopes are not truly ANCF elements. However, in *dncm* formulation [28], there is not much practical difference between elements with and without slopes because all elements can be described by a contiguous and uniform set of parameters. To the best knowledge of the authors, there have been only a few studies that considered “truly ANCF elements.” Among them is the recent study of the authors on 3D solid brick elements with slopes [30]. Wei and Shabana [31] also proposed a new approach for computational fluid dynamics using ANCF solid finite elements with slopes.

The purpose of the present study was the development of an effective complement to the previously proposed eight-node solid element [30] by reformulating the simplest tetrahedral element, which uses translations of the nodes as nodal coordinates, as an isoparametric ANCF element for use together with the solid brick element. Several types of tetrahedral

elements were considered in [1]. The conventional tetrahedral element with additional nodes on its faces was formulated by Argyris [32]. More recent studies considered conventional tetrahedral elements with improved properties [33, 34]. The selection of the particular element to be reformulated using ANCF and the details of its development are presented in the following sections.

This paper is organized as follows: In Sect. 2, the digital nomenclature code *dncm* for the systematic description of elements is briefly discussed. This notation was used throughout the present study because the authors considered it to be convenient, especially in situations when many different elements had to be described. Section 3 presents explanation of how the *dncm* code can be used for the automated generation of shape functions for arbitrary 3D solid elements. Furthermore, in Sect. 4, some of the nuances of the derivation of the equations of motion are discussed. Finally, Sect. 5 is devoted to the numerical simulation of statics and dynamics benchmarks, the validation of the element and illustration of its performance.

## 2 Digital nomenclature *Dncm* to describe finite elements

Many finite elements are presently used for modeling and numerical simulation in diverse areas of physics. Unfortunately, there is no universal system for the designation of elements to reflect their kinematic properties. The complete description of an element is tedious and not convenient for use, and the specification of the numbers of nodes or degrees of freedom of an element is also not sufficient to uniquely describe the element. All commercial FEA softwares usually use their own element names such as BEAM189, PLANE25, or SOLID164 in ANSYS [35]. Such nomenclatures are, however, still not sufficiently informative. A universal naming system that reflects the topological and kinematic properties of the elements would be more helpful. The introduction of such systematic classification was attempted by Dmitrochenko and Mikkola [28]. The proposed digital nomenclature code denoted by *dncm* can be used to describe a wide variety of finite elements by using four digits:

- digit *d* is the local dimension of the element: value  $d = 1$  is used for beams;  $d = 2$  for plates or shells, and  $d = 3$  for solids;

- digit *n* shows the number of nodes of the element;
- digit *c* represents nodal coordinates understood as the number of derivatives of the field variables vector  $\mathbf{r}$  starting from 0th derivative, i.e., variable  $\mathbf{r}$  itself; typical values of parameter *c* used in this paper are:

$c = 1$  for any *d* means that a single value  $\mathbf{r}$  of the field variable is used;

$c = 2$  for case  $d = 1$  corresponds to nodal variables  $\mathbf{r}, \frac{\partial \mathbf{r}}{\partial x}$ ;

$c = 3$  for case  $d = 2$  corresponds to nodal variables  $\mathbf{r}, \frac{\partial \mathbf{r}}{\partial x}, \frac{\partial \mathbf{r}}{\partial y}$ ;

$c = 4$  for case  $d = 3$  corresponds to nodal variables  $\mathbf{r}, \frac{\partial \mathbf{r}}{\partial x}, \frac{\partial \mathbf{r}}{\partial y}, \frac{\partial \mathbf{r}}{\partial z}$ .

- digit *m* shows the multiplicity of field variables, i.e., the number of components in vector  $\mathbf{r}$ . For elements with  $m = 1$  the fourth digit can be omitted.

An element described by *dncm* code has  $n \times c \times m$  degrees of freedom. In the present study, the *dncm* nomenclature code is mostly used for designating the elements. The procedure for deriving new elements using the nomenclature code is described in [28].

Figure 1 represents a few examples of using *dncm* nomenclature for different finite elements. We note that any code *dncm* corresponds to a certain abstract element. However, some of them are outside the practical interest of structural mechanics.

## 3 Formulation of 3D element

### 3.1 Tetrahedral solid element

The solid brick element 3843, which has slopes and uses an incomplete cubic polynomial, was previously developed by the authors. This element was derived as a 3D generalization of 1D beam and 2D plate with slopes using a straightforward approach [30]. The similar development of a tetrahedral element with slopes encounters certain difficulties.

The element 3443 would be a complete four-node kinematic analogue of the solid brick element 3843. However, for the case of four nodes ( $n = 4$ ) with the same coordinate sets for all the vertex nodes, and which includes translations and three spatial derivatives ( $c = 4$ ), the total number of nodal vectors would

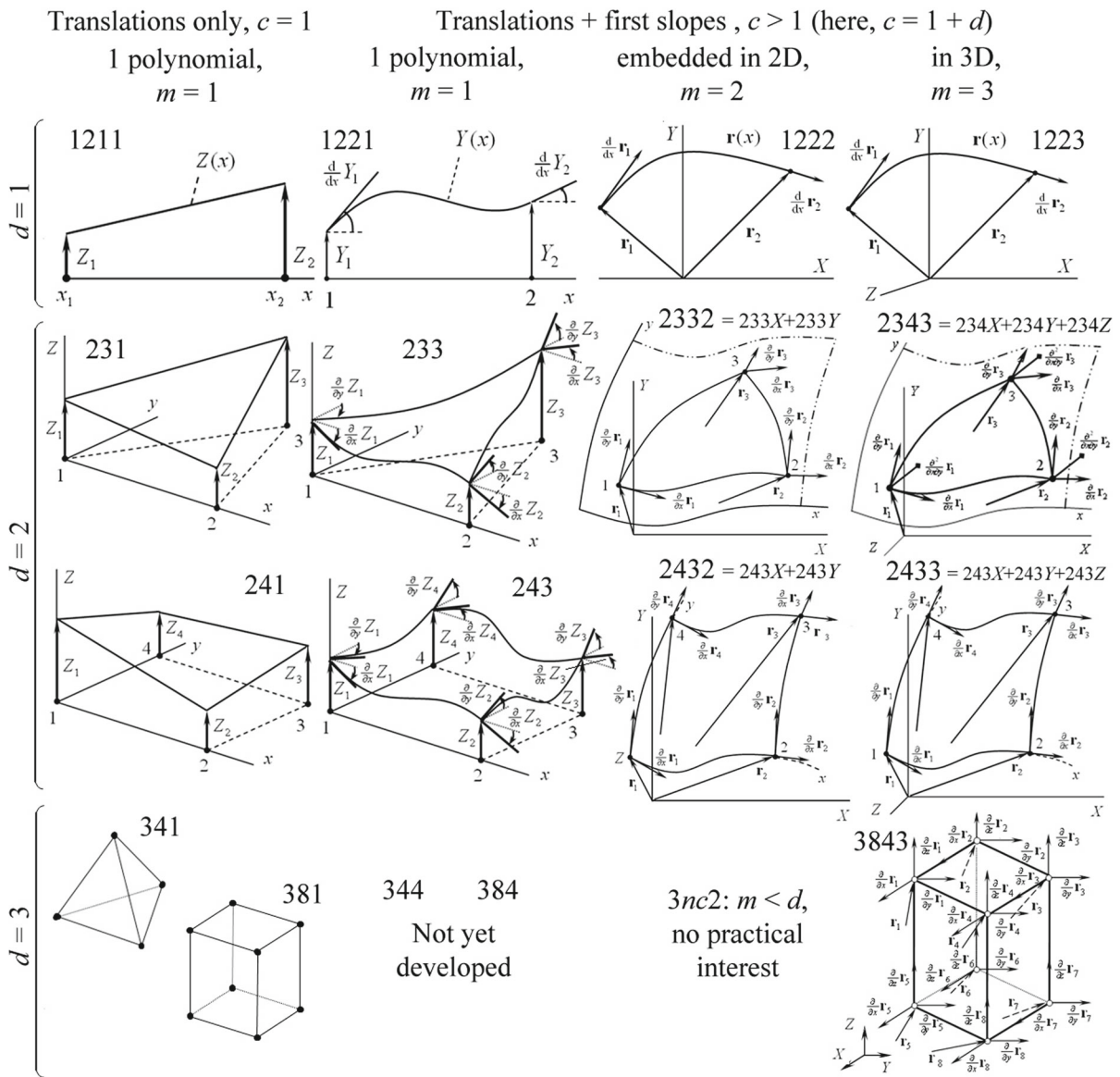
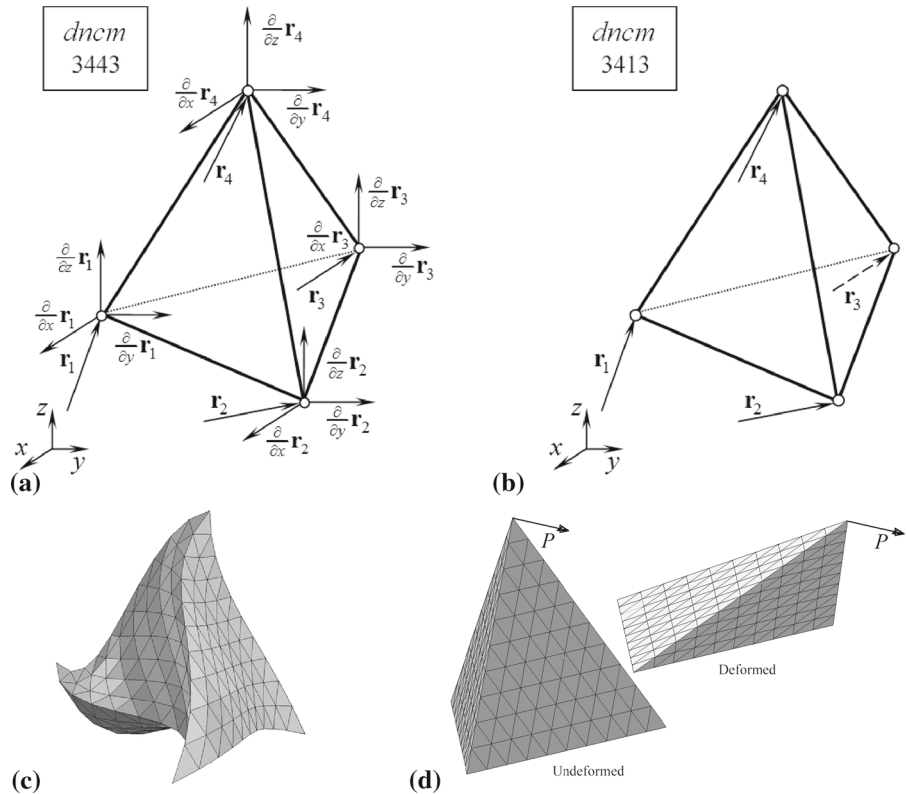


**Fig. 1** Locally  $d$ -dimensional  $n$ -node elements with  $c$  nodal  $m$ -vector per node

be  $n \cdot c = 4 \cdot 4 = 16$  terms, while the complete cubic polynomial should have included 20 terms. This would lead to degeneration of the element. It is therefore necessary to extend the element kinematics. One way of doing this is to introduce additional nodes with translational sets of coordinates on the element faces. However, we reserve this idea for implementation in a following paper.

The simplest tetrahedral element that possesses only translational degrees of freedom (Fig. 2b) can be denoted by 3413 because it has nodes only on its vertices and all the nodes have the same translational set of coordinates. From practical point of view, this means that edges and faces of the simplest tetrahedral element 3413 remain straight after deformation, while

**Fig. 2** Elements 3443 (a) and 3413 (b) and examples of their deformed shapes (c, d)



the curvature of the edges and faces of a more complex element 3443 is determined by its slopes. Examples of the deformed shapes of these elements are presented in Fig. 2c, d.

It is obvious that the abilities of the element 3413 to represent deformed shapes are limited, compared to the element 3443 employing slopes since the slopes facilitate the prevention of the shear locking effect in bending problems and make a model comprising a small number of elements capable to represent large deformations. This issue was discussed in the study [36], devoted to the two-dimensional elements 2412 and 2432. At the same time, one should keep in mind that the ANCF elements employing slopes and having many degrees of freedom have very high computational complexity, which can be justified by the possibility of using a fewer number of elements in a model. However, for many problems when nuances of shape require developing large models, a solid tetrahedral element without slopes has definite advantages due to its versatility and higher performance. That is why the element 3413 is still of a practical interest.

### 3.2 Numerical computation of shape functions for 3D solid elements

The interpolation polynomial for the general case of a 3D solid element ( $d = 3$ ) with  $n$  nodes and  $c$  coordinates per node can be expressed as follows:

$$\begin{aligned}
 Z^{3nc}(x, y, z) &= \sum_{k=0}^{D-1} a_{k+1} x^{\alpha_{Dk}} y^{\beta_{Dk}} z^{\gamma_{Dk}} = \\
 &= \underbrace{\{ x^{\alpha_{D0}} y^{\beta_{D0}} z^{\gamma_{D0}} \dots x^{\alpha_{D,D-1}} y^{\beta_{D,D-1}} z^{\gamma_{D,D-1}} \}}_{\mathbf{x}(x,y,z)} \\
 &\cdot \underbrace{\{ a_1 \dots a_D \}^T}_{\mathbf{a}} = \mathbf{x}(x, y, z) \cdot \mathbf{a} \tag{1}
 \end{aligned}$$

In Eq. (1), the exponential coefficients  $\alpha_{Dk}$ ,  $\beta_{Dk}$ , and  $\gamma_{Dk}$  are used. They should be obtained from the  $D^{\text{th}}$  row of the matrix given in Fig. 3, where  $D = n \times c$  is the number of unknown coefficients  $a_k$  of the polynomial.

The unknown coefficients can be determined from a system of linear equations obtained by the evaluation of the polynomial  $Z^{3nc}(x, y, z)$  and its proper derivatives at the nodal points  $(x_i, y_i, z_i)$ . The system of linear equations can be generally described as follows:

$$i = 1, \dots, n; j = 0, \dots, c - 1; l = (i - 1)c + j + 1 \frac{\partial^{\alpha_{Dj} + \beta_{Dj} + \gamma_{Dj}} Z^{3nc}(x, y, z)}{\partial x^{\alpha_{Dj}} \partial y^{\beta_{Dj}} \partial z^{\gamma_{Dj}}} \Big|_{\substack{x=x_i \\ y=y_i \\ z=z_i}}$$

$$\equiv \sum_{k=0}^{D-1} \underbrace{(\alpha_{Dk})_{-\alpha_{Dj}} (\beta_{Dk})_{-\beta_{Dj}} (\gamma_{Dk})_{-\gamma_{Dj}} x_i^{\alpha_{Dk} - \alpha_{Dj}} y_i^{\beta_{Dk} - \beta_{Dj}} z_i^{\gamma_{Dk} - \gamma_{Dj}}}_{W_{l,k+1}} a_{k+1} = z_l \text{ or } \mathbf{W} \cdot \mathbf{a} = \mathbf{z}. \tag{2}$$

The differentiation of the left-hand side of Eq. (2) results in a reduction in the exponents of the polynomial terms in Eq. (1) by  $\alpha_{Dj}, \beta_{Dj}$ , and  $\gamma_{Dj}$ , as well as in multiplication of the terms by Pochhammer's falling factorial  $(\alpha_{Dk})_{-\alpha_{Dj}}, (\beta_{Dk})_{-\beta_{Dj}}$ , and  $(\gamma_{Dk})_{-\gamma_{Dj}}$ :

$$(\alpha)_{-r} = \underbrace{\alpha \times (\alpha - 1) \times \dots \times (\alpha - r + 1)}_{r \text{ multiplicands}}$$

$$= \prod_{i=0}^{r-1} (\alpha - i) = \begin{cases} \frac{\alpha!}{(\alpha-r)!} & \text{if } \alpha \geq r; \\ 0 & \text{if } \alpha < r. \end{cases} \tag{3}$$

Equation (2) is a linear system of equations, which a constant square matrix  $\mathbf{W}$ , which can be solved for vector of unknown coefficients  $\mathbf{a}$ . After substitution of this vector to Eq. (1), the shape functions of the finite element take the form:

$$Z^{3nc}(x, y, z) = \sum_{i=1}^{\dim E} \sum_{j=0}^{\dim E_i - 1} \sum_{k=0}^{D-1} \overbrace{x^{\alpha_{Dk}} y^{\beta_{Dk}} z^{\gamma_{Dk}}}^{(\mathbf{x}(x))_k} \underbrace{\sum_{l=1}^D W_{k+1,l}^{-1} Z_l}_{s_i^{3nc}(x)}, \tag{4}$$

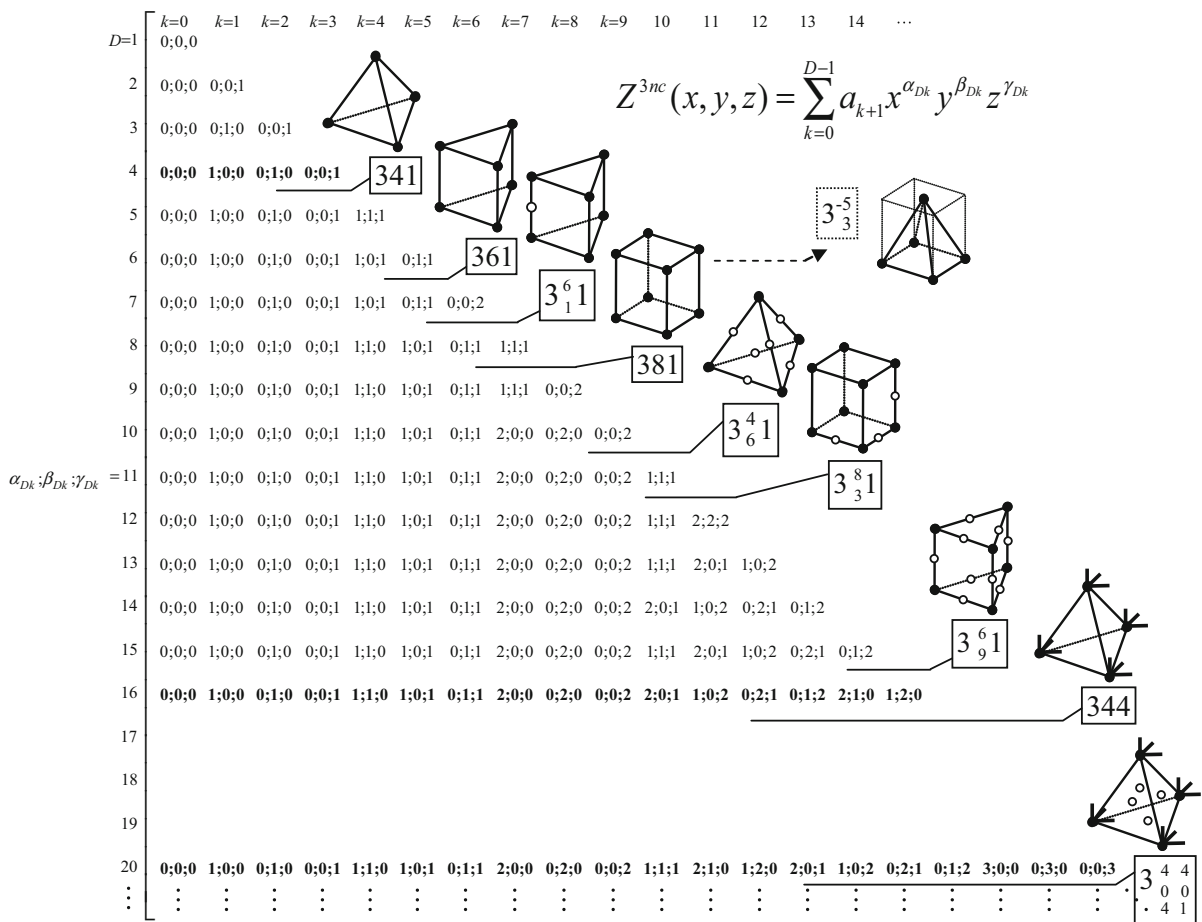


Fig. 3 Exponential coefficient matrix

where the row matrix has shape functions  $\mathbf{s}^{3nc}$  and the column matrix has nodal coordinates  $\mathbf{z}$ . Equation (4) can be written as follows:

$$Z^{3nc}(x, y, z) = \underbrace{\mathbf{x}(x, y, z) \cdot \mathbf{W}^{-1}}_{\mathbf{s}^{3nc}(x,y,z)} \cdot \mathbf{z} = \mathbf{s}^{3nc}(x, y, z) \cdot \mathbf{z}. \tag{5}$$

The simplest tetrahedral element 3413 has only four nodes and employs only nodal positions. The application of the above formulas produces the following shape functions, the so-called volume (or tetrahedral) coordinates:

$$s_{i,0}^{341}(x, y, z) = \det \begin{vmatrix} 1 & x & y & z \\ 1 & x_j & y_j & z_j \\ 1 & x_k & y_k & z_k \\ 1 & x_l & y_l & z_l \end{vmatrix} \bigg/ \det \begin{vmatrix} 1 & x_1 & y_1 & z_1 \\ 1 & x_2 & y_2 & z_2 \\ 1 & x_3 & y_3 & z_3 \\ 1 & x_4 & y_4 & z_4 \end{vmatrix}, \tag{6}$$

where the indices  $i, j, k$ , and  $l$  are given by the cyclic permutation  $\{i, j, k, l\} = \Theta(1, 2, 3, 4)$ .

For more complicated elements, the complexity of the shape functions makes their explicit expressions difficult to display. Hence, Eqs. (1)–(5) were implemented as numerical procedures and used in this study to compute the terms of the equations of motion as described below. The shape functions were calculated by using the numerical procedure, which is described in detail for an arbitrary element in studies [24] and [28]. For the simplest tetrahedral element considered in the study, the use of this procedure is not quite justified because of the simplicity of the element. However, for 3D solid and plate/shell elements with slopes the advantage of numerical computation of shape functions is more obvious. Implementing the numerical procedures for the element 3413 has provided a background for developing more complex elements, in particular the element 3443—a tetrahedron with slopes.

### 3.3 Numerical computation of structural matrices of 3D solid elements

A continuum mechanics approach is used to calculate the vector of elastic forces. The energy accumulated in the volume of the deformed element is determined by the following integral:

$$U = \frac{1}{2} \iiint_V \boldsymbol{\varepsilon}^T \cdot \mathbf{E} \cdot \boldsymbol{\varepsilon} \, dx dy dz, \tag{7}$$

where

$$\boldsymbol{\varepsilon} = \left\{ \begin{array}{l} \frac{\mathbf{r}'_x \cdot \mathbf{r}'_x - 1}{2}, \quad \frac{\mathbf{r}'_y \cdot \mathbf{r}'_y - 1}{2}, \quad \frac{\mathbf{r}'_z \cdot \mathbf{r}'_z - 1}{2}, \\ \mathbf{r}'_x \cdot \mathbf{r}'_y, \quad \mathbf{r}'_y \cdot \mathbf{r}'_z, \quad \mathbf{r}'_z \cdot \mathbf{r}'_x \end{array} \right\} \tag{8}$$

is a Voigt representation of the nonlinear Green–Lagrange strain tensor, and  $\mathbf{E}$  is a matrix of elastic constants including Young’s modulus  $E$  and Poisson’s ratio  $\nu$ :

$$\mathbf{E} = \frac{E}{(1 + \nu)(1 + 2\nu)} \begin{bmatrix} 1 - \nu & \nu & \nu & 0 & 0 & 0 \\ \nu & 1 - \nu & \nu & 0 & 0 & 0 \\ \nu & \nu & 1 - \nu & 0 & 0 & 0 \\ 0 & 0 & 0 & \frac{1-2\nu}{2} & 0 & 0 \\ 0 & 0 & 0 & 0 & \frac{1-2\nu}{2} & 0 \\ 0 & 0 & 0 & 0 & 0 & \frac{1-2\nu}{2} \end{bmatrix}. \tag{9}$$

The integral in expression (7) can be calculated analytically or numerically. For most of the elements employing the ANCF, the analytical expressions are extremely cumbersome. This causes additional difficulties and dramatically increases the computational costs. The vector of the generalized elastic forces  $\mathbf{Q}$  can be determined as a gradient of the strain energy  $U$ :

$$\mathbf{Q} = \frac{\partial U}{\partial \mathbf{e}}, \tag{10}$$

where  $\mathbf{e} = (\mathbf{r}_1^T, \mathbf{r}_2^T, \mathbf{r}_3^T, \mathbf{r}_4^T)^T$  is the vector of nodal coordinates of the element.

### 4 Equations of motion

The equations of motion are formulated as follows:

$$\mathbf{M}\ddot{\mathbf{e}} + \mathbf{Q} = \mathbf{Q}_e, \tag{11}$$

where  $\mathbf{M}$  is the mass matrix,  $\ddot{\mathbf{e}}$  is the vector of the nodal accelerations,  $\mathbf{Q}$  is the vector of the nonlinear elastic nodal forces, and  $\mathbf{Q}_e$  is the vector of the external forces.

The mass matrix can be obtained using the expression for the kinetic energy of the element, obtained by integrating all the material point velocities squared in the volume domain of the undeformed element:

$$T = \frac{1}{2} \iiint_V \rho \mathbf{r}^T \cdot \dot{\mathbf{r}} \, dx dy dz, \tag{12}$$

where  $\dot{\mathbf{r}}$  is the velocity of an arbitrary point in the element, and  $\rho$  is the material density. The mass matrix is defined as follows:

$$\mathbf{M} = \iiint_V \rho \mathbf{S}^T \cdot \mathbf{S} \, dx dy dz, \tag{13}$$

where  $\mathbf{S}$  is the matrix of the shape functions. The mass matrix remains constant under an arbitrary large displacement and rotation of the element.

The vector of elastic forces and mass matrix were calculated numerically. For integration over the interior of a tetrahedron, the quadrature rules described in [37] were used. The final values of the terms of equations of motion for Eqs. (10) and (13) can be written as follows:

$$\mathbf{Q} = \Delta \sum_{i=1}^N w_i \frac{\partial \boldsymbol{\varepsilon}}{\partial \mathbf{e}_{(i)}} \cdot \mathbf{E} \cdot \boldsymbol{\varepsilon}_{(i)}, \quad \mathbf{M} = \rho \Delta \sum_{i=1}^N w_i \mathbf{S}_{(i)}^T \mathbf{S}_{(i)}. \tag{14}$$

In Eq. (14),  $N$  is the number of nodes in the quadrature rule,  $w_i$  is the weight coefficient,  $\Delta$  is the tetrahedron volume, lower indices ( $i$ ) refer to matrices associated with node  $i$  of the quadrature. The generalized elastic forces were calculated using a one-point quadrature rule; for the mass matrix, a four-point quadrature rule was used. This is because the term  $\frac{\partial \boldsymbol{\varepsilon}}{\partial \mathbf{e}_{(i)}}$  is constant for element 3413, while the term  $\mathbf{S}_{(i)}^T$  is of higher order.

In the simulation of static problems, a damping factor was introduced into the equations of motion using a simple approach based on the theory of the vibration of a system with a single degree of freedom. The magnitude of the damping factor for a non-periodic motion was determined from the period of the free vibrations,  $T$ , which was preliminarily evaluated for the models. The equation of motion was then solved in the form

$$\mathbf{M} \cdot \ddot{\mathbf{e}} + \mathbf{D} \cdot \dot{\mathbf{e}} + \mathbf{Q}(\mathbf{e}) = \mathbf{Q}_e, \tag{15}$$

where

$$\mathbf{D} = \alpha \mathbf{M}, \quad \alpha = \frac{4\pi}{T}. \tag{16}$$

This approach seems to be applicable to cases in which the purpose of the damping is simply to suppress inexpedient oscillations. A rigid body motion that could be damped out was not observed in these problems.

### 5 Numerical examples

To validate the performance and accuracy of the element, several statics and dynamics benchmarks were simulated. The numerical solutions were compared with those obtained by other ANCF finite elements and commercial CAE software. The MATLAB software was used to perform several numerical simulations using ANCF elements. The equations of motion were integrated using the solver *ode45*. The solver was selected based on the Young’s modulus of the model material according to the recommendations given in [24].

We note that MATLAB is only suitable for relatively simple ANCF simulations using models with small numbers of elements. For models comprising hundreds of elements or more, the use of a compiled code instead of the MATLAB interpreter is highly recommended because of the computational complexity of the ANCF problems. In this study, all simulations were performed on the computer with Intel(R) Core(TM) i5-4570 CPU @ 3.20GHz with 16 GB RAM under Windows 7.

#### 5.1 Bar tension

This simple statics benchmark was simulated as a dynamics problem, wherein critical damping was introduced into the system as expressed by Eqns. (15) and (16). The bar, which had a length  $L = 0.5$  m and rectangular cross section  $a \times b = 0.1 \times 0.1$  m, was hinged on its top face and subjected to a large tension. The Young’s modulus  $E$ , Poisson’s ratio  $\nu$ , and material density  $\rho$  were  $2 \times 10^5$  Pa, 0.3, and  $7800 \text{ kg/m}^3$ , respectively. An axial load of 120 N was distributed along the edges of the bottom face of the bar. The displacements of two cross sections (the bottom face and middle cross section) were evaluated for models with different numbers of elements along the length of the bar (Figs. 4 and 5). In all cases, these displacements were considered as the displacements of the cross-sections’ centroids and were calculated as the average displacements of nodes in the cross-sections’ corners.



**Fig. 4** Displacement of the middle cross section of the bar for different FE models

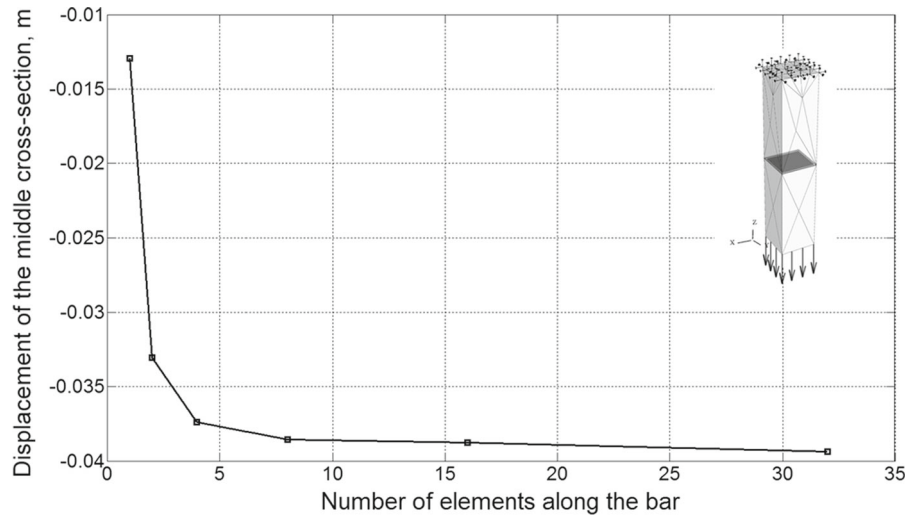
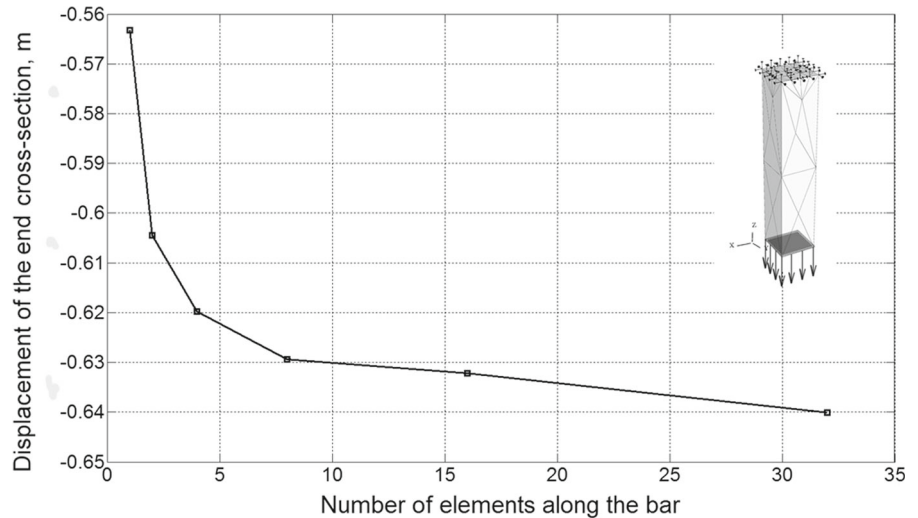


**Fig. 5** Displacement of the free-end cross section of the bar for different FE models



The solution obtained using ABAQUS software for this problem using a model with a fine element mesh comprising 5000 elements of the type C3D8 (a general-purpose linear brick element, fully integrated) gave the displacements of  $-0.038$  m for the middle cross section and  $-0.069$  m for the free-end cross section. For the middle cross section, the solutions are in good agreement. For the free-end cross section, the difference can be explained by lower stiffness of the model with a finer mesh and local singularity at the points of load application.

### 5.2 Motion of a falling pendulum

The flexible pendulum is a well-known and frequently simulated benchmark used for the validation of new

finite elements [16,24,30]. The kinematic scheme of the pendulum is shown in Fig. 6a. The constraints were imposed on the translational degrees of freedom at the nodes on one of the edges of the pendulum as shown in the figure. The dimensions of the pendulum  $L \times b \times h$  were  $0.5 \times 0.1 \times 0.1$  m, and the Young's modulus  $E$ , Poisson's ratio  $\nu$ , and material density  $\rho$  were 2 MPa, 0.3, and  $7800 \text{ kg/m}^3$ , respectively. The pendulum fell from its vertical position. A damping factor  $\alpha$  of 1 was used for the as expressed by Eqs. (15), (16). Figure 6b shows the change of the vertical ( $Z$ ) coordinate of the centroid  $C$  of the pendulum free-end cross section in time for different models. The bold continuous curve represents the results obtained using the model formed from 69 elements with  $dncm$  3413 (described in this paper); the thin continuous curve represents the results

**Fig. 6** Kinematic scheme and Z-coordinate of the pendulum’s free-end cross-sectional centroid

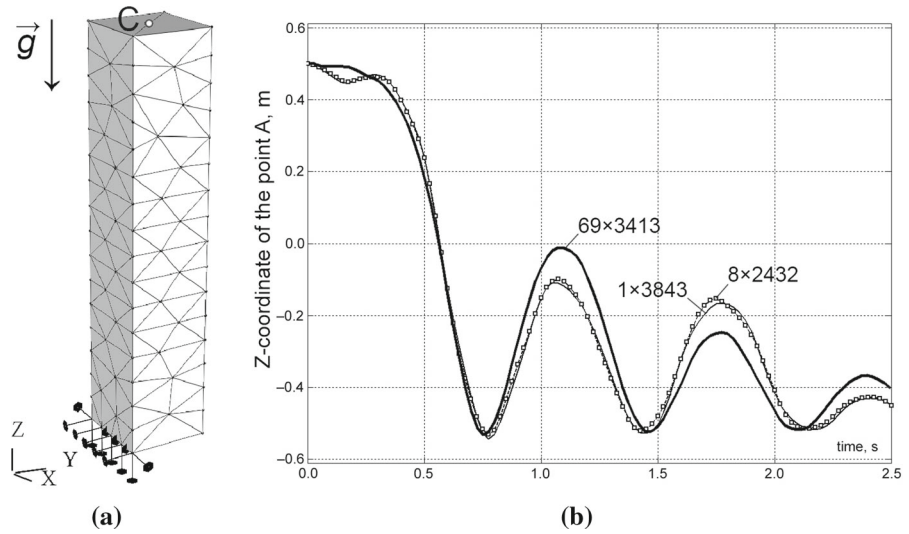


**Table 1** Models for simulating a flexible pendulum (*dncm* 3413, see Fig. 7)

Model	I	II	III	IV	V
Number of elements along pendulum’s length	1	2	4	8	16
Total number of elements	24	48	48	96	507

obtained using the single element 3843 [30]; and the square markers represent the results obtained using the two-dimensional model formed from eight 2432 plate elements [24] in two dimensions.

It can be observed from the figure that the curves are quite close to each other for the first 0.75 s and are thereafter slightly diverged. This can be explained by the absence of slopes in the 3413 elements and their subjection to the shear locking effect. However, the large number of elements used in the model mitigated the effect of locking.

For illustrating the convergence of the element, the same problem was simulated for the models comprising different numbers of elements. The damping was not introduced in this simulation. The vertical displacement of point A at the free end of the pendulum was evaluated. Six different models were used. Five of them were comprised different numbers of elements 3413 (Table 1), whereas the sixth one included eight elements 3843 [30] and was used for obtaining the reference solution, which is shown in Fig. 7 by the square-marked curve. A typical time required for MATLAB simulation of 1 second of motion of the model comprising 96 tetrahedral elements (Model

IV) was about 109 seconds. This gives some representation about the element efficiency in this particular implementation.

### 5.3 Motion of flexible ellipsograph

The motion of a heavy flexible beam under the action of gravity was simulated. The length  $L$  of the beam was 1 m, and the height  $h$  and width  $b$  of its rectangular cross section were 0.02 and 0.01 m, respectively. The model parameters were as follows: the density  $\rho = 3900 \text{ kg/m}^3$ , the Young’s modulus  $E = 10^6 \text{ Pa}$ , and the Poisson’s ratio  $\nu = 0.3$ . The vertical displacement of the left end of the beam and the horizontal displacement of the right end were constrained as shown in the top left corner of Fig. 8. The motion of the model during 1 s was simulated.

The model of the beam comprised 76 tetrahedral elements (*dncm* 3413). The solution was compared with those obtained using two solid brick elements with slopes (*dncm* 3843) [30], two plate elements with slopes (*dncm* 2432) [24], and forty well-known beam elements with slopes (*dncm* 1222) [2], respectively. In

**Fig. 7** Vertical (Z) coordinate of point A on the pendulum for different models (see Table 1)

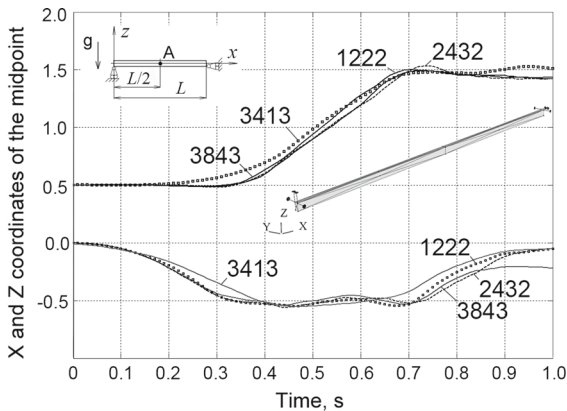
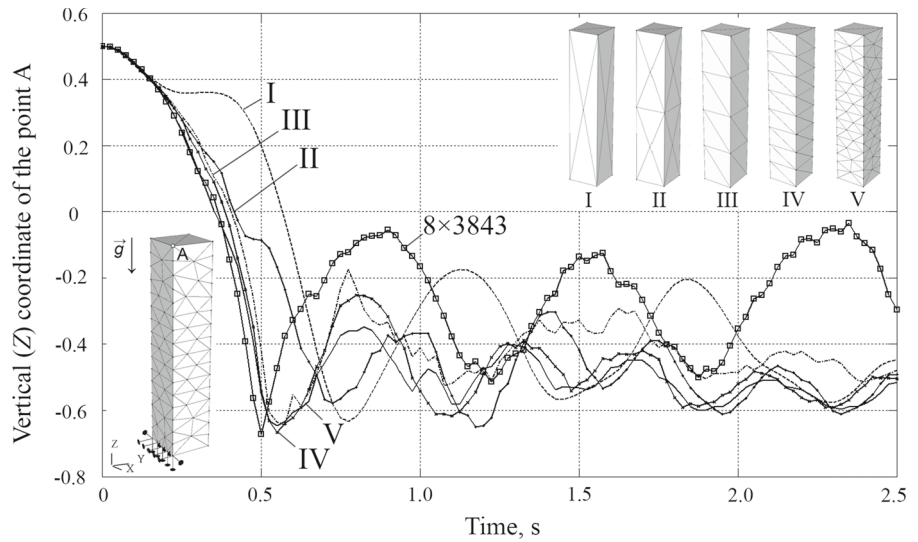


**Fig. 8** X and Z coordinates of point A in time, calculation scheme, and the model

Fig. 8, the bottom group of curves represents the vertical (z) coordinate of the centroid of the middle cross section (point A) of the beam during its motion. The change in the horizontal (x) coordinate of point A is described by the upper group of curves.

It can be seen that, despite the significantly larger number of the simplest tetrahedral elements used for this simulation, the displacement of the midpoint of the element 3413 was smaller than that of the higher-order elements. This fact shows that the element 3413 experienced shear locking and should therefore be used with definite caution when dealing with bending problems. Nevertheless, bearing in mind the low computational complexity in using the element, the results are quite satisfactory.

### 5.4 Practical application

The element 3413 was also validated by using it to solve a practical problem of a real technical object, namely the elastic polymer block in the center coupler draft gear of a railway vehicle. The block is identified as part PMKP-110 [38], which was developed by LLC Diprom. This device is widely used on railways in the Russian Federation and other countries of the former USSR. PMKP-110 is mounted on a railway freight car to absorb impacts during motion and when coupling cars. The design, CAD model, and general view of PMKP-110 are presented in Fig. 9.

The pressing wedge (5), the frictional wedges (4) that make contact with the support plate (6), the moving friction plates (3), and the stationary friction plates (2) with wear-proof metal-ceramic elements are all assembled in the housing (1). The plate is supported by a set of five elastic PVC blocks (7 and 8) delimited by the alignment plates (10). The device is held by the clamp bolt with a nut (9) and has a design stroke of 110 mm. The force from the coupler is transferred through the pressing plate to the pressing wedge, which moves together with the side friction wedges (4) and the support plate (6). In the first stage of an impact, the central frictional section operates, and frictional forces are generated on the surfaces of the side wedges and the stationary friction plates. When the support plate has been displaced by a certain value, the second stage commences, wherein the movable plates, stationary plates,

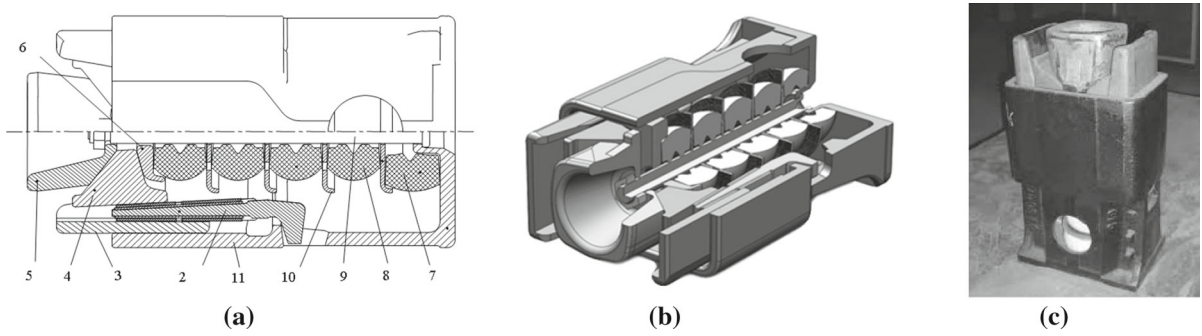


**Fig. 9** Design (a), CAD model (b), and general view (c) of PMKP-110

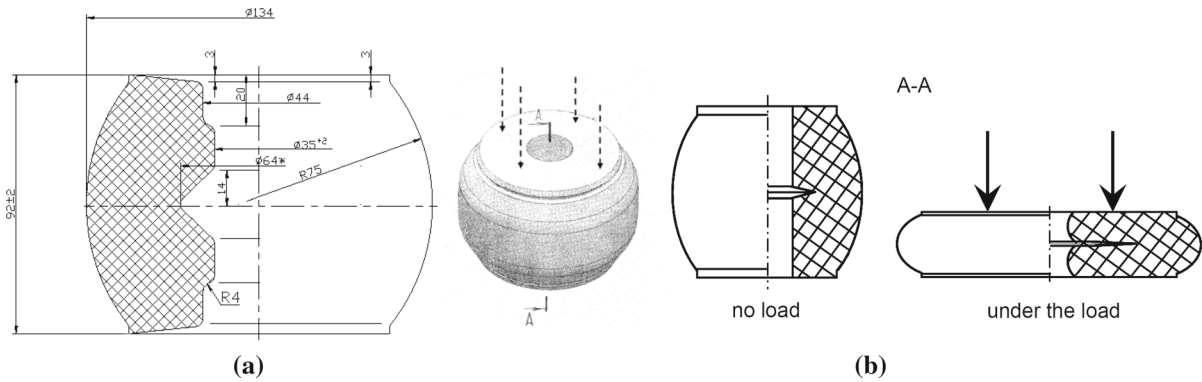


**Fig. 10** Design drawing (a) and schematic of the deformation of the polymer block (b) used in PMKP-110

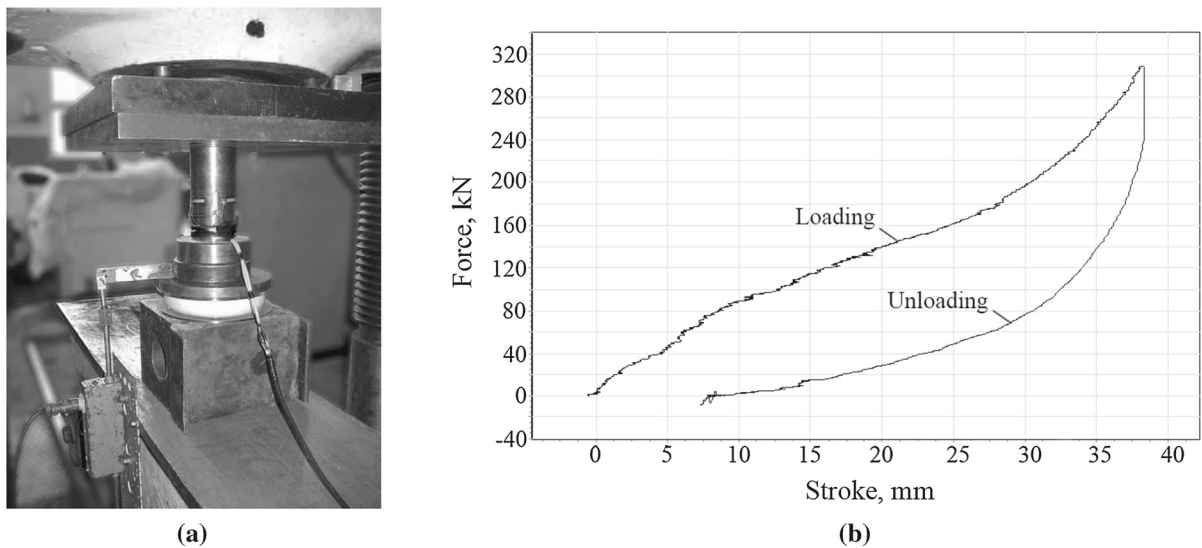


**Fig. 11** Force–stroke diagram of the single PVC element obtained by experiment

and side surfaces of the haul start operating, and the overall resistance to the applied pressure is increased. The energy spent for the compression of the draft gear is

expended partially for compression of the PVC blocks and, to a far greater degree, for friction between the parts.

**Fig. 12** Finite element model of PVC block (a) and its deformation under the load (b)

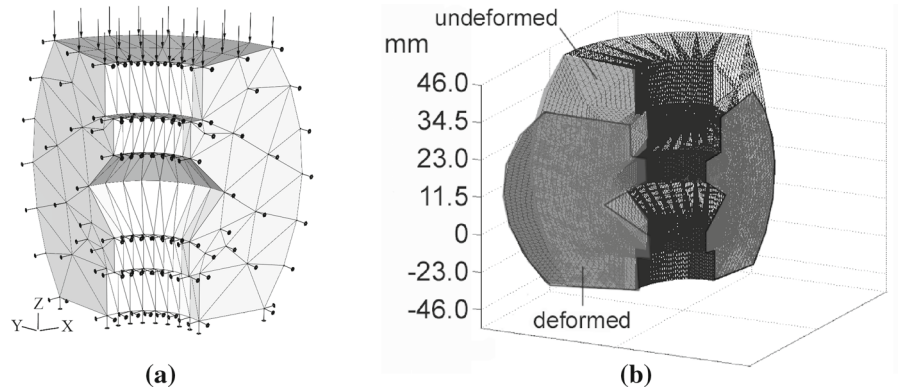


**Table 2** Comparison of simulated and experimental stroke–force diagrams

Top face displacement (stroke) (mm)	Compressive force (kN)		Error (%)
	Experiment	ANCF	
10	85	86	−1.18
15	113	115	−1.77
20	140	143	−2.14
25	162	167	−3.09

The key feature of PMKP-110 is the use of five polymer (PVC) blocks (position 8 in Fig. 9a) instead of the metal spring used in many similar devices. The use of an elastic polymer block affords better force characteristic and increases the elastic capacity of the device. In addition, the damping properties of the polymer significantly reduce the self-excited frictional vibrations that follow a shock compression. The design drawing of the polymer element and a schematic of its deformation by a normal operation impact are shown in Fig. 10.

The processes that take place in the shock absorber are too complicated to be described here, and a detailed simulation of the processes is beyond the scope of the present study. However, the deformation of a single polymer block among the set used in the absorber can be properly observed by experiments. For test purposes, a single PVC block was subjected to a compressive load of up to 310 kN Fig. 11a. The stroke–force diagram is shown in Fig. 11b.

It can be seen that the loading and unloading branches of the force–stroke diagram are different and produce a hysteresis loop, which is determined by the specific properties of the specimen material. A physically accurate numerical simulation of this test is a challenging problem because it requires accounting for the nonlinear properties of the material as well as the sim-

ulation of a step-by-step loading, which are beyond the purposes of this study. Nevertheless, it was possible to approximately simulate the test and obtain basic quantitative results, particularly the maximum displacement under the given load. These results validate the possibility of applying element 3413 to real-world problems involving geometrically nonlinear compression.

5.4.1 Simulation of compression test

A finite element model comprising 234 nodes and 816 tetrahedral elements was developed. Owing to the symmetry of the problem, a quarter of the specimen was considered and the corresponding boundary conditions were applied (Fig. 12). All three components of the displacement of the nodes of the lower face were constrained, but friction between the nodes and the supporting surface was not taken into consideration.

Kinematic loading was used for the simulation to produce equal displacements of the nodes on the top face of the model corresponding to the conditions of the experiment. The vertical coordinate ( $z$ ) of the nodes on the top face was gradually varied at time intervals of  $T$  to produce the particular displacement of the top face corresponding to a given stroke as determined by experiment (Fig. 11):

$$z = z_0 - \Delta z \cdot \cos\left(\pi \frac{t}{T}\right), \quad (17)$$

where  $z_0$  is the initial value of the coordinate,  $\Delta z$  is the displacement of the node, and  $T$  is the time interval of the application of the load. Large displacements of the top face of the block (greater than 25 mm) cause the closure of the gap between the recess edges, as shown in Fig. 10. Simulation of this closure requires accounting for contact in the solving procedures, which is currently not implemented in our code. For this reason, the maximum value of the displacement was limited by 25 mm, which guarantees that the gap will not be closed. That is, a part of the loading curve was simulated. The Young's modulus  $E$  and Poisson's ratio  $\nu$  were 6.8 MPa and 0.35, respectively. The stress at each selected node was then calculated, and the total compressive force corresponding to the displacement was determined as the product of the calculated stress and the area of the top face. The comparison of simulated and experimental results is given in Table 2.

The calculated values of the compressive force are in good agreement with those determined by experiment. From an engineering point of view, the accuracy of the results is satisfactory.

## 6 Conclusion

The simplest solid tetrahedral finite element possessing translations of nodes as sets of nodal coordinates (*dncm* code 3413) were reformulated by absolute nodal coordinate formulation. This tetrahedral shape of the element makes it versatile for modeling members of engineering structures with complex shapes. The small number of the degrees of freedom of the element 3413 enables good performance when applied to problems of structural dynamics and makes the use of the element promising. The accuracy and convergence of the element were validated by statics and dynamics benchmarks. The tetrahedral shape of the element makes it versatile for modeling members of engineering structures with complex shapes. This was illustrated in simulation of a practical problem.

**Acknowledgements** This research was supported by Agency for Defense Development under the contract UD150022GD, National Research Foundation of Korea(NRF) grant 2016R1A2B 2015794, and the 2016 KU Brain Pool of Konkuk University.

## References

- Zienkiewicz, O.C., Taylor, R.L.: The Finite Element Method, Solid and Fluid Mechanics, vol. 2, 4th edn. McGraw-Hill Book, New York (1991)
- Shabana, A.A.: Dynamics of Multibody Systems, 3rd edn. Cambridge University Press, New York (2005)
- Shabana, A.A.: Definition of the slopes and the finite element absolute nodal coordinate formulation. *Multibody Syst. Dyn.* **1**(3), 339–348 (1997)
- Gerstmayr, J., Shabana, A.: Analysis of thin beams and cables using the absolute nodal coordinate formulation. *Nonlinear Dyn.* **45**(1–2), 109–130 (2006)
- Wu, G., He, X., Pai, F.: Geometrically exact 3D beam element for arbitrary large rigid-elastic deformation analysis of aerospace structures. *Finite Elem. Anal. Des.* **47**(4), 402–412 (2011)
- Yoo, W.-S., Dmitrochenko, O., Park, S.-J., Lim, O.-K.: A new thin spatial beam element using the absolute nodal coordinates: application to a rotating strip. *Mech. Based Des. Struct. Mach.* **33**(3–4), 399–422 (2005)
- Dmitrochenko, O.: Finite elements using absolute nodal coordinates for large-deformation flexible multibody dynamics. *J. Comput. Appl. Math.* **215**(2), 368–377 (2008)
- Gerstmayr, J., Matikainen, M., Mikkola, A.: A geometrically exact beam element based on the absolute nodal coordinate formulation. *Multibody Syst. Dyn.* **20**(4), 359–384 (2008)
- Nachbagauer, K., Gruber, P., Vetyukov, Y., Gerstmayr, J.: A spatial thin beam finite element based on the absolute nodal coordinate formulation without singularities. In: Proceedings of the ASME 2011 Int. Design Eng. Techn. Conf. & Computers and Information in Eng. Conf. IDETC/CIE 2011. Washington, DC, USA, 2011.08.28–31. (2011) by ASME
- Nachbagauer, K., Gruber, P., Vetyukov, Y., Gerstmayr, J.: Structural and continuum mechanics approaches for a 3D shear deformable ANCF beam finite element: application to static and linearized dynamic examples. *J. Comput. Nonlinear Dyn.* **8**(2), 021004 (2012)
- Nachbagauer, K., Pechstein, A.S., Irschik, H., Gerstmayr, J.: A new locking-free formulation for planar, shear deformable, linear and quadratic beam finite elements based on the absolute nodal coordinate formulation. *Multibody Syst. Dyn.* **26**(3), 245–263 (2011)
- Schwab, A. L., Meijaard, J. P.: Comparison of three-dimensional flexible beam elements for dynamic analysis: classical finite element formulation and absolute nodal coordinate formulation. *J. Comput. Nonlinear Dyn.* **5**(1), 011010 (2009). doi:10.1115/1.4000320
- Bauchau, O., Han, S., Mikkola, A., Matikainen, M.: Comparison of the absolute nodal coordinate and geometrically exact formulations for beams. *Multibody Syst. Dyn.* **32**, 67–85 (2014)
- Vohar, B., Kegl, M., Ren, Z.: Implementation of an ANCF beam finite element for dynamic response optimization of elastic manipulators. *Eng. Optim.* **40**(12), 1137–1150 (2008)
- Matikainen, M., Schwab, A., Mikkola, A.: Comparison of two moderately thick plate elements based on the absolute nodal coordinate formulation. *Multibody dynamics 2009, ECCOMAS Thematic Conference*. In: Arczewski, K.,

- Frączek, J., Wojtyra M. (eds.), Warsaw, Poland, 29 June–2 July (2009)
16. Dmitrochenko, O., Pogorelov, D.: Generalization of plate finite elements for absolute nodal coordinate formulation. *Multibody Syst. Dyn.* **10**(1), 17–43 (2003)
  17. Dmitrochenko, O., Mikkola, A.: Two simple triangular plate elements based on the absolute nodal coordinate formulation. *J. Comput. Nonlinear Dyn.* **3**(4), 041012 (2008)
  18. Dmitrochenko, O., Mikkola, A.: Shear correction of a thin plate element in absolute nodal coordinates. In: Proc. of 8th World Congr. On Comp. Mech. (WCCMS) and 5th Eur. Congr. on Computat. Meth. in Appl. Set and Eng. (ECCOMAS 2008). 2008.06.30–04. Venice. Italy. ISBN 978–84–96736–55–9. p. 127
  19. Dmitrochenko, O., Mikkola, A.: Shear correction for thin plate finite elements based on the absolute nodal coordinate formulation. In: Proceedings of ASME 2009 IDETC/CIE 2009. 2009.08.30–02. San Diego. California. USA. 1–9
  20. Hyldahl, P., Mikkola, A., Balling, O.: A thin plate element based on the combined arbitrary Lagrange–Euler and absolute nodal coordinate formulations. In: Proceedings of the Institution of Mechanical Engineers, Part K: Journal of Multi-body Dynamics, (2013)
  21. Shi, W., Park, H., Chung, C., Baek, J., Kim, Y., Kim, C.W.: Load analysis and comparison of different jacket foundations. *Renew. Energy* **54**, 201–210 (2013)
  22. Langerholc, M., Slavič, J., Boltežar, M.: A thick anisotropic plate element in the framework of an absolute nodal coordinate formulation. *Nonlinear Dyn.* **73**(1–2), 183–198 (2013)
  23. Olshevskiy, A., Dmitrochenko, O., Dai, M.D., Kim, C.W.: The simplest 3-, 6- and 8-noded fully-parameterized ANCF plate elements using only transverse slopes. *Multibody Syst. Dyn.* **34**(1), 23–51 (2015)
  24. Olshevskiy, A., Dmitrochenko, O., Lee, S.S., Kim, C.W.: A triangular plate element 2343 using second-order absolute-nodal-coordinate slopes: numerical computation of shape functions. *Nonlinear Dyn.* **74**(3), 769–781 (2013)
  25. Yamashita, H., et al.: Continuum mechanics based bi-linear shear deformable shell element using absolute nodal coordinate formulation. *J. Comput. Nonlinear Dyn.* (2014). doi:[10.1115/1.4028657](https://doi.org/10.1115/1.4028657)
  26. Gerstmayr, J., Sugiyama, H., Mikkola, A.M.: Review on the absolute nodal coordinate formulation for large deformation analysis of multibody systems. *J. Comput. Nonlinear Dyn.* **8**, 031016 (2013). doi:[10.1115/1.4023487](https://doi.org/10.1115/1.4023487)
  27. Gallagher, R.H.: Finite element analysis: Fundamentals. Prentice-Hall Civil Engineering and Engineering Mechanics Series. Prentice-Hall, Englewood Cliffs (1975)
  28. Dmitrochenko, O., Mikkola, A.: Extended digital nomenclature code for description of complex finite elements and generation of new elements. *Mecha. Based Des. Struct. Mach. Int. J.* **39**(2), 229–252 (2011)
  29. Kübler, L., Eberhard, P., Geisler, J.: Flexible multibody systems with large deformations and nonlinear structural damping using absolute nodal coordinates. *Nonlinear Dyn.* **34**, 31–52 (2003)
  30. Olshevskiy, A., Dmitrochenko, O., Kim, C.W.: Three-dimensional solid brick element using slopes in the absolute nodal coordinate formulation. *J. Comput. Nonlinear Dyn.* **9**, 021001 (2014)
  31. Wei, C., Shabana, A.: A total Lagrangian finite element approach for computational fluid dynamics based on absolute nodal coordinates formulation. In: The 3rd Joint International Conference on Multibody System Dynamics, The 7th Asian Conference on Multibody Dynamics. June 30–July 3, 2014, BEXCO, Busan, Korea
  32. Argyris, J.H., Fried, I., Sharpf, D.W.: The TET 20 and TEA8 elements for the matrix displacement method. *Aeronaut. J. R. Aeronaut. Soc.* **72**, 618–623 (1968)
  33. Lo, S.H., Ling, C.: Improvement on the 10-node tetrahedral element for three-dimensional problems. *Comput. Methods Appl. Mech. Eng.* **189**, 961–974 (2000)
  34. Taylor, R.L.: A Mixed-Enhanced Formulation for Tetrahedral Finite Elements. Report No. UCB/SEMM-99/02
  35. ANSYS, Inc., ANSYS® Academic research, release 11.0, Help system, coupled field analysis guide, (2008)
  36. Olshevskiy, A., Dmitrochenko, O., Kim, C.W.: Three- and four-noded planar elements using absolute nodal coordinate formulation. *Multibody Syst. Dyn.* **29**(3), 255–269 (2013)
  37. Dufva, K., Shabana, A.: Analysis of thin plate structures using the absolute nodal coordinate formulation. In: Proc. of the Inst. of Mech. Eng., Part K: J. of Multibody Dynamics. December 1 1(219), 345–355 (2005)
  38. Kehlin, B.H., Boldyriev, O.P., Ivanov, O.V., Stupin, D.O.: Improving the efficiency of combined friction of shock-absorbing devices on the basis of the PMK-110A. *Science and Transport Progress. Bull. Dnipropetrovsk Natl. Univ. Railw. Transp.* **5**, 85–95 (2004)